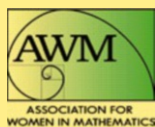


Association for Women in Mathematics Series

Ami Radunskaya · Rebecca Segal
Blerta Shtylla *Editors*

Understanding Complex Biological Systems with Mathematics



 Springer

Simulations of the Vascular Network Growth Process for Studying Placenta Structure and Function Associated with Autism



Catalina Anghel, Kellie Archer, Jen-Mei Chang, Amy Cochran, Anca Radulescu, Carolyn M. Salafia, Rebecca Turner, Yacoubou Djima Karamatou, and Lan Zhong

Abstract Placenta chorionic surface vascular networks differ in individuals at-risk for autism compared to controls in terms of longer, straighter, thicker vessels; less branching; smaller changes in flow directions; and better coverage to the

C. Anghel
University of California Davis, Davis, CA, USA
e-mail: catalina.anghel@alum.utoronto.ca

K. Archer
The Ohio State University, Columbus, OH, USA
e-mail: archer.43@osu.edu

J.-M. Chang (✉)
California State University Long Beach, Long Beach, CA, USA
e-mail: jen-mei.chang@csulb.edu

A. Cochran
University of Wisconsin, Madison, WI, USA
e-mail: cochran4@wisc.edu

A. Radulescu
SUNY New Paltz, New Paltz, NY, USA
e-mail: radulesa@newpaltz.edu

C. M. Salafia
Placental Analytics, LLC., New Rochelle, NY, USA

R. Turner
Scion, Riccarton, Christchurch, New Zealand
e-mail: Rebecca.Turner@scionresearch.com

D. Yacoubou Djima
Amherst College, Amherst, MA, USA
e-mail: kyacouboudjima@amherst.edu

L. Zhong
University of Delaware, Newark, DE, USA
e-mail: lanzhong@udel.edu

© The Author(s) and the Association for Women in Mathematics 2018
A. Radunskaya et al. (eds.), *Understanding Complex Biological Systems with Mathematics*, Association for Women in Mathematics Series 14,
https://doi.org/10.1007/978-3-319-98083-6_7

145

placental boundary. What mechanism(s) could drive these differences and how these mechanisms would impact blood transport has not been widely investigated. We used a Monte-Carlo simulation to mimic three mechanisms for controlling vascular growth: vessels grow faster and longer, terminate more frequently before branching, and flow directions are more tightly controlled in the at-risk simulations. For each mechanism, we analyzed simulated vascular networks based on structural properties and blood flow, assuming Poiseuille's law and distensible vessels. Our simulations showed that none of these mechanisms alone could reproduce all structural properties of vascular networks in placentas identified as at-risk for autism. Terminating vessels more frequently or growing longer vessels could each reproduce longer vessels and less branching, but not greater boundary coverage or smaller changes in flow directions. As for their influence on blood flow, longer vessels and less branching have large, opposing effects on network function. Networks with longer vessels are less efficient in terms of slower flow rates and higher total network volume; in contrast, networks with less branching are more efficient. Our results suggest either these mechanisms work together to drive observed differences in vascular networks of at-risk individuals by balancing their impacts on network function; or another mechanism not considered here might drive these differences.

Keywords Placentas · Autism · Vascular networks · Blood flow · Simulations

1 Introduction

Biomarkers of autism spectrum disorder (ASD) are believed to be a linchpin in understanding what causes ASD, by pointing to specific biological pathways that are involved [1]. Such biomarkers are found as early on in a childhood development as pregnancy and frequently traced to the placenta, the locus of maternal–fetal interactions. Placentas differ in morphology and structure in individuals with ASD and/or at-risk for ASD compared to controls [4, 16, 18, 19] and may be modified by maternal stress and illness, well-known factors in ASD [2]. While the placenta has a clear role in ASD, what remains unclear is whether this role is one of mediator, root cause, by-product, and/or association. Simply put, do placental changes contribute to the development of ASD or are these changes simply indicative of some other factor that contributes to ASD? A small step towards answering these questions is determining how the placenta could function as a mediator or a root cause.

Placental function centers on a fetal vascular network of veins and arteries which transfers oxygen, nutrients, and biochemicals from the maternal blood into the fetal blood. The fetal vascular network in the placenta begins and ends where the umbilical cord, made up of two primary arteries and a vein, inserts into the placenta. Following the primary arteries leads to successively smaller branches throughout the chorionic plate (the region in the placenta near the fetus) and culminates in *chorionic villi* or *villous trees*, where oxygen and nutrients are transferred. Substrates are then

carried back to the umbilical cord along veins that approximately mirror the arterial network.

Broadly, a placenta could cause ASD, if it was unable to transport enough oxygen (hypoxia), nutrients, and biochemicals for the fetal brain to grow and develop properly. Placental-derived serotonin, for example, is hypothesized to be lower in individuals with ASD at a critical time in fetal brain growth and development [20]. A placenta could mediate ASD, if other factors were to limit the placenta's ability to transport oxygen and nutrients. Inflammation from maternal illness, a prime suspect in ASD [11, 14, 15], is known to impact vascular growth in general [6] and hence, may impact the placental vascular network in particular. Moreover, a placenta's function is tied to its structure and morphology, which has known distinctive features in individuals with ASD or at-risk for ASD compared to controls, such as a more constrained chorionic plate [19] and fetal vascular networks with thicker and straighter vessels that branch less frequently than the controls [4].

In what follows, we examine the potential role for the placenta as a cause or a mediator of ASD. Through mathematical and computational approaches, we first explore simple mechanisms for growing placental vascular networks and altering overall network structure in Sect. 2. Then in Sect. 3, we use our simulated networks to study how changes in vascular networks impact fetal blood flow in the placenta and subsequently, to relate our simple mechanisms to a placenta's ability to transfer oxygen and nutrients from the mother to the fetus. We conclude by relating our insights back to ASD and proposing specific testable hypotheses about the placenta's role in ASD. Ultimately, we aim to identify potential mechanisms by which the placenta may influence the behavioral abnormalities clinically observed within the autistic spectrum. Numerical implementations were done in MATLAB without special packages, and all of the simulations were rendered in real-time on typical notebook computers. Interested readers are encouraged to contact the authors for the codes.

2 Mechanisms for Placental Vascular Growth

In this section, we investigate simple mechanisms for growing placental vascular networks, with an emphasis on identifying mechanisms that could reproduce empirical properties of placental vascular networks in ASD. Empirical properties reported in this study were computed from placentas sampled from two independently collected cohorts, the Early Autism Risk Longitudinal Investigation (EARLI) [13] and the National Children's Study (NCS). Protocols were approved by the pertinent Institutional Review Boards and this study deals with de-identified data only. EARLI is an autism enriched-risk pregnancy cohort that focuses on prenatal and early life periods of children who have biological siblings already diagnosed with ASD. EARLI children are at an increased risk for ASD, thereby denoted as an *at-risk*

Table 1 Left: parameters and constants used to simulate vascular networks. Right: seven sets of parameter combinations chosen to systematically examine how certain parameters influence vascular growth and function

Symbol	Description	Value(s)
R	Placenta radius	9.25 cm
L_1	Mean first generation growth length	1.4 cm
L_2	Mean second generation growth length	1.8 cm
c	No. of first generation vessels	2
N_g	No. of generations	8–10
x_0	Umbilical cord insertion	(0, 0)
θ	Restriction angle	$[\frac{\pi}{4}, \frac{\pi}{2}]$
t	Growth fraction, generation $g > 1$	[0.2, 0.6]
L_g	Growth length, generation $g > 1$	Eq. (1)–(2)
f	Angle reduction factor	[0, 1]
α	Termination fraction	[0.5, 0.7]
d_g	Vessel diameter, generation $g \geq 1$	Eq. (3)–(4)

Set	t	L_g	f	α	d_g
Baseline	0.4	N/A	0.6	0.5	Eq. (3)
2	0.5	N/A	0.6	0.6	Eq. (3)
3	N/A	Eq. (1)	0.6	0.5	Eq. (3)
4	N/A	Eq. (2)	0.6	0.5	Eq. (3)
5	0.4	N/A	1.0	0.5	Eq. (3)
6	0.4	N/A	0.6	0.7	Eq. (3)
7	0.4	N/A	0.6	0.5	Eq. (4)

cohort. On the other hand, NCS is a population-based cohort with pregnancies at unknown risk for ASD. NCS was designed to study environmental influences on child health and development and it enlisted participants without a bias towards risks and diagnoses of autism. Placentas in NCS are used here as an unselected normal-risk baseline, thereby denoted as a *control* cohort. We used a total of 201 NCS placentas and 89 EARLI placentas in our simulations.

Our approach is to use simple algorithms and a few key parameters to simulate and control the growth process in theoretical vascular networks. To simulate the growth process, we built upon a Monte-Carlo algorithm described by Wang et al. [22] which was applied to placentas in the work of Clark et al. [5]. To control the growth process, we modified (1) vessel growth speed, (2) angles between connected vessels, and (3) termination of vessel growth. These three features are represented by key parameters, controlled within a biological range. Other parameters such as placenta radius were fixed throughout the simulations. See Table 1 for the values selected in the experiments. Each theoretical network assessed in Sect. 2.4 includes (1) the locations where two or more vessels connect (branching points), (2) locations where vessels end (terminal points), and (3) descriptive information on vessels (e.g., radii and lengths). We then measured properties of our theoretical vascular networks, such as average distance from terminated vessels to the placenta boundary and total rotation angle along vascular trajectories, to determine how changes in the growth process could give rise to placental vascular networks characteristic of ASD.

2.1 A Simple Mechanism for Vascular Growth

Following Wang et al. [22] and Clark et al. [5], we simulated the growth of a placental vascular network under the guiding principle that vessels should cover the maternal side of the placenta, so oxygen and nutrients can be transferred throughout this area. This area is represented mathematically by a set of seed points $A(0, 0)$ drawn uniformly at random to cover a two-dimensional circular region with radius R . A circular region is chosen for its simplicity.

The first step of generating vessels begins, similarly to the real process, with the insertion of the umbilical chord. We denote the insertion point by x_0 and for simplicity, assume it is the center/origin $(0, 0)$ of the circular region. At the insertion point, the umbilical cord most often branches into two vessels. Hence, the first two vessels are specified to grow from the insertion point with a distance L . The angle between the parent and children vessels is set to be a uniform random variable in $[60^\circ, 180^\circ]$. The endpoints of the two vessels are denoted by $x(1, 1)$ and $x(1, 2)$. Each point in the seed set, $A(0, 0)$, is then placed into one of the two sets, $A(1, 1)$ and $A(1, 2)$, based on which endpoint is closer.

The second step of generating vessels is to use the line connecting the origin x_0 to the branch $x(1, 1)$ to partition the seed set $A(1, 1)$ into two new sets $A(2, 1)$ and $A(2, 2)$. Similarly, the line connecting the origin x_0 to $x(1, 2)$ is used to partition $A(1, 2)$ into two subsets $A(2, 3)$ and $A(2, 4)$. We then grow four new vessels from the first generation branches: two vessels from $x(1, 1)$ towards the centroids of the seed sets $A(2, 1)$ and $A(2, 2)$ and two vessels from $x(1, 2)$ towards the centroids of $A(2, 3)$ and $A(2, 4)$. In general, step g of the generative vessels is defined iteratively: for $k = 1, \dots, 2^g$,

1. Partition $A(g - 1, k)$ into two sets $A(g, 2k - 1)$ and $A(g, 2k)$ using the line connecting $x(g - 1, k)$ to the centroid of $A(g - 1, k)$;
2. Grow two new vessels from $x(g - 1, k)$ to the centroids of $A(g, 2k - 1)$ and $A(g, 2k)$;
3. Stop growth of vessels at points $x(g, 2k - 1)$ and $x(g, 2k)$ that lie a distance L away from $x(g - 1, k)$.

We continue to grow vessels for a fixed number of generations N_g . The branching process is illustrated in Fig. 1.

2.2 Vascular Network Model Parameters

We now turn to investigate how growth mechanisms influenced the overall structure of the simulated vascular network. The empirical data was used to define some parameters of interest, some parameters were varied, and other parameters were measured as outcomes from the simulations. Our key parameters were allowed to vary within ranges and rules informed by the empirical data. We used different

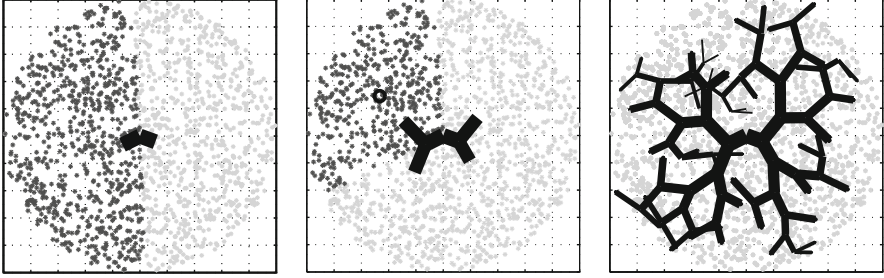


Fig. 1 Illustration of a simple growth model. Stars represent seed points. Left: Branches of the first generation. The dark grey stars represent the seed set corresponding to the left branch A(1, 1). Center: Branches of the first and second generation. The seed set has been split in two with the top left branch growing towards the centroid marked by the black circle. Right: Completed tree with eight generations

invariant measures to characterize the system which we simulated based on the key parameters. We studied the dependence of these measures on the primary parameters, and we compared with empirically driven hypotheses. All predefined parameters and constants are detailed in Table 1.

When possible, parameters were derived from the data (Fig. 2). For example, three parameters: placenta radius R , average first generation vessel length L_1 , and average second generation vessel length L_2 were chosen to be the average between the corresponding measures for at-risk individuals and controls. The number of first generation branches was set to 2, since about 70% of the placentas in our data sets have two branches in their first generation. Parameter L_g ($g > 2$) was chosen to depend linearly on g , and was therefore fitted to the best fit line (in a least-squares sense) to either curve from generations 3–10 in Fig. 2c for vessel length in controls (Eq. (1)) and at-risk (Eq. (2)) individuals, respectively:

$$L_g := (-0.09g + 2.12) \text{ cm} \quad (1)$$

and

$$L_g := (-0.10g + 2.30) \text{ cm} \quad (2)$$

Similarly, a vessel diameter d_g for generation $g \geq 1$ was determined by fitting a fourth-degree polynomial in generation g to either curve in Fig. 2g for vessel diameter in controls (Eq. (3)) and at-risk (Eq. (4)) individuals, respectively:

$$d_g = 8.19 \times 10^{-5}g^4 - 0.00256g^3 + 0.0302g^2 - 0.168g + 0.483; \quad (3)$$

and

$$d_g = 7.13 \times 10^{-5}g^4 - 0.00230g^3 + 0.0285g^2 - 0.166g + 0.499. \quad (4)$$

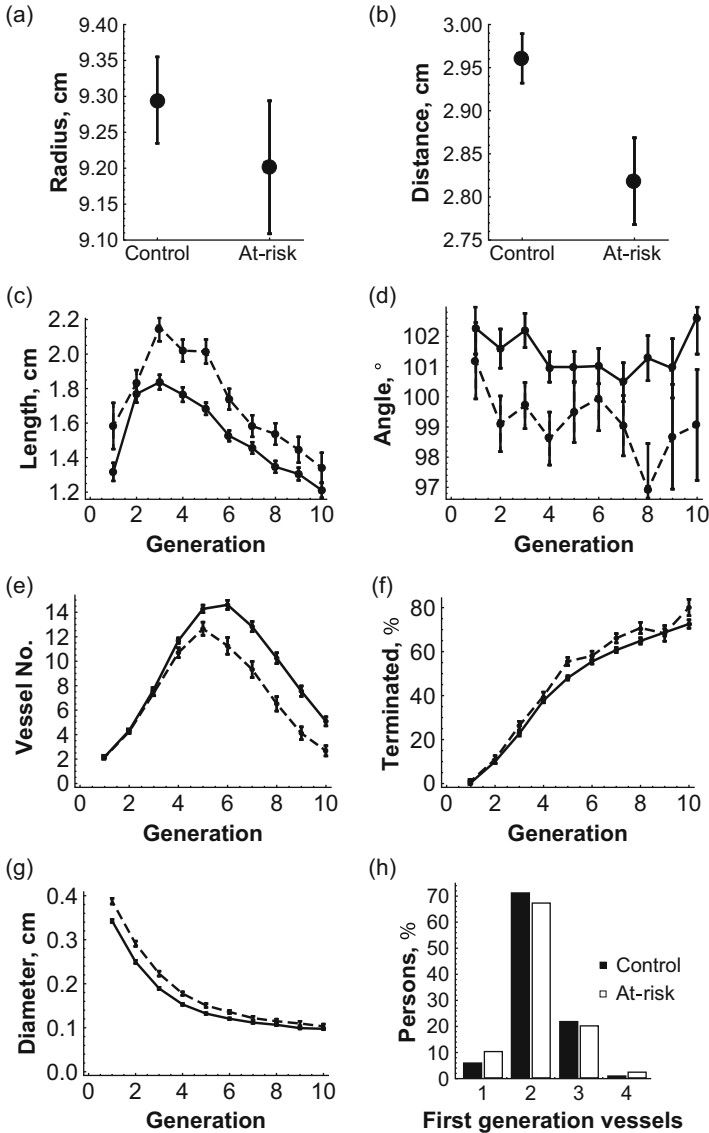


Fig. 2 Placenta data from at-risk and controls. (a) average placenta radius, (b) distance from terminated vessels to placenta boundary, (c) vessel length, (d) angle between branching vessels, (e) number of vessels, (f) percentage of vessels terminated, (g) vessel diameter, and (h) number of placentas with a specific number of first generation vessels. The control group are represented by the solid lines, and the at-risk group by the dashed line. Averages are taken within a generation and individual placentas and then averaged over each risk cohort. Error bars represent standard errors for a participant group

Many curves could be used to model and achieve comparable results; fourth-degree polynomials were used here for their accuracy ($r^2 > 0.99$).

2.3 *Candidate Mechanisms for Vascular Growth in ASD*

We further modified the simple growth mechanism, described in Sect. 2.1, to better represent actual placentas and to introduce three ways vascular growth might be modified in ASD.

Vessels Grow Faster The simple growth mechanism uses a fixed length for every vessel in the vascular network, a feature which does not accurately capture real placentas. Vessels that grow at different speeds, defined as vessel length per generation, could lead to vascular networks with different properties. We considered two possible growth mechanisms to introduce variable vessel lengths for generations $g > 1$. The first is to grow a vessel for a fraction t of the distance from the original branching point towards the centroid of its respective seed set. The second is to grow each vessel within a generation step g for a uniform random length with mean L_g and range $0.4L_g$. In each of the two approaches, first generation vessels grow for a uniform random distance of mean L_1 and range $0.4L_1$.

Vessels Terminate More Frequently Vessel growth often terminates before branching in a real placenta. This termination could be an important factor in vascular growth, reflecting, say, limited resources in one particular area of the placenta. Therefore, we terminated the branching process for a vessel that either left the convex hull of its corresponding seed points or had a corresponding seed set with a ratio of branches to seed points that exceeded $1/8$. In addition, we randomly terminated the branching process with a probability $\alpha/(1 + e^{-(g-\hat{g})})$ at each generation step $g > 1$, where $\hat{g} = 5$ in the exponent $-(g - \hat{g})$ is the average simulated number of generations. With this logistic function, termination would have little impact at the start of the branching process and the amount of the growth near the end is also limited. Parameter $\alpha \in [0, 1]$ is referred to as the “termination fraction.” This will force the remaining vessels to redirect, affecting the general geometry of the vascular tree. The centroids are then updated to accommodate the new seed points. The addition of seed points does result in some seed sets that have concave polygon shapes, or that span branches from previous branch generations. This may not be realistic, making this aspect of the research an area for future development.

Angles Between Connected Vessels Are More Tightly Controlled The simple growth model determines branching angles based on the centroid locations, but a real placenta may be more restricted in its branching angles. For example, we would not expect an angle larger than 90° between a vessel and any of its branching vessels so that blood flow does not make such a sudden turn. The density of the tissue

surrounding the vascular tree could also limit the branching angle, whereby higher-density tissue produces shallower (more acute) branching angles compared to lower-density tissue which allows more freedom for wider branching angles. If φ is the angle between the flow direction in a parent vessel and the flow direction in either one of the children vessels at a branching point, then we simulated the control effect by decreasing φ to $\varphi - f(\varphi - \theta)$ for any $\varphi \geq \theta$, where $\theta \in [0, 2\pi]$ and $f \in [0, 1]$ are constants/parameters. The threshold θ is called the “restriction angle” and the factor f is called the “angle reduction factor.”

Based on these candidate mechanisms, certain key parameters were varied to measure their influence on vascular growth with those ranges given in Table 1. To this end, we simulated 50 networks for each of the seven sets of parameters/growth rules (right panel of Table 1). For each set, we measured average distance of terminated vessels to placenta boundary, vessel length, branching angle, and percentage of vessels terminated at each generation step. The significance and effects of these parameters are described and illustrated in the rest of this section. The simulated network invariants will be compared against the empirical at-risk and control cases illustrated in Fig. 2. One of our aims is to understand which key parameters such as branch length and control angle account for which of the network differences which are significantly different between the two empirical groups. Note that the vessel diameter does not influence the growth process; however, it is important when analyzing blood flow and pressure in Sect. 3.

2.4 Results of the Impact of Vascular Growth on Network Structure

Here we present the results of varying key parameters in the simulation, such as vessel number, vessel growth speed (measured via a growth factor or the vessel lengths), branching angle, and termination fraction on network invariants, such as average distance of terminated vessels to the boundary and global rotation angle (a measure of the tortuosity in the network). Example simulated vascular networks are shown in Fig. 3. Figure 4 shows the impact of controlling vessel growth speed, and Fig. 5 shows the impact of controlling the angle between branching vessels and the frequency of vessel termination.

Growth Factor t Our first growth mechanism—branch length depends on distance to its seed set’s centroid—benefits from having only a few parameters and simple explanations for why certain branches are longer: they grow faster per generation and/or start farther from the seed set. This growth mechanism also provides a way to illustrate how placenta growth and vascular growth are coupled. Namely, one can use the convex hull of the centroids of seed sets at generation step g to simulate the boundary of the growing placenta (See Appendix 1). In this case, the boundary of the placenta is redefined by the centroids of the new partition of the

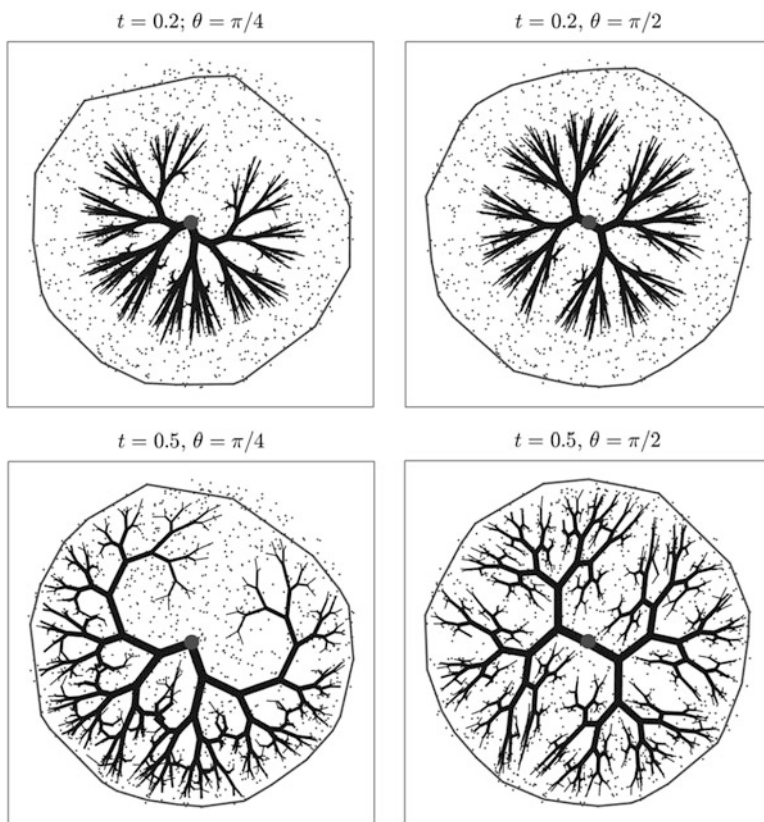


Fig. 3 Comparing properties of the simulated vascular tree between parameter values (growth speed and angle restriction). The top row shows vascular trees for slow growth ($t = 0.2$), for more restricted angles ($\theta = \pi/4$, left) and for less restricted angles ($\theta = \pi/2$, right). The bottom row shows vascular trees for faster growth ($t = 0.5$), for more restricted angles ($\theta = \pi/4$, left) and for less restricted angles ($\theta = \pi/2$, right). In all cases, ϕ was used as a sharp threshold (i.e., $f = 1$)

seed set and approaches the boundary of the a priori given seed set over generation steps. Meanwhile, new vessels grow out in the direction of this boundary (the new generation of centroids), but may branch before reaching the boundary.

Notice that a higher growth fraction leads to a vascular network with vessels that are longer and offering increased coverage to the placenta boundary compared to a lower growth fraction. This phenomenon is evidenced in Figs. 3 and 4. Notably, both features are empirical characteristic of at-risk individuals (Fig. 2b, c); hence, a bigger growth fraction could explain why these two features are observed. However, in Fig. 4, we also observe that a higher growth fraction leads to larger branching angles and fewer terminated vessels, contrary to what is observed for empirical at-risk individuals in Fig. 2d, f. Furthermore, this growth mechanism fails to capture the general trend in vessel length by generation of both controls and at-risk individuals.

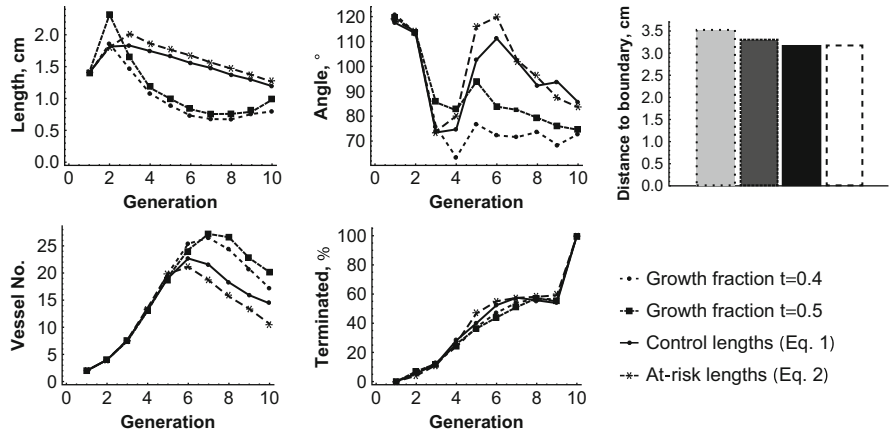


Fig. 4 Impact of various growth mechanisms and parameters. Fifty networks were simulated for different sets of parameters to estimate average vessel length, branching angles, number of vessels, vessel termination, and distance from terminated vessels to the placenta boundary. Here, the angle reduction factor, f , is set to 1 and the termination fraction, α , is set to 0.5

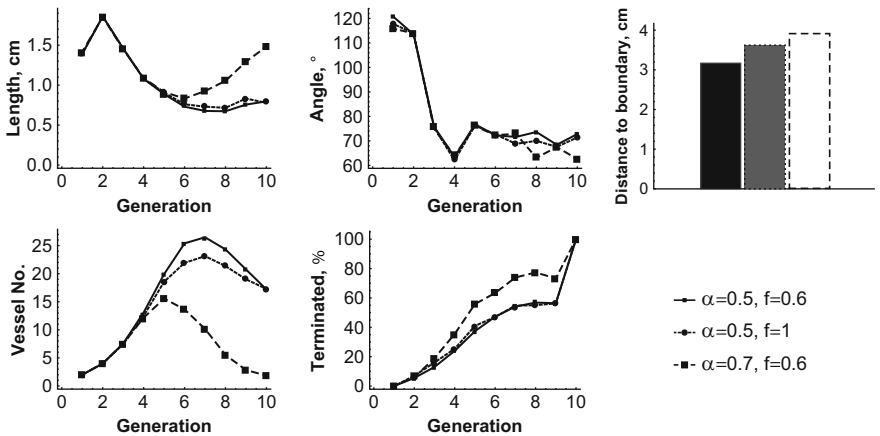


Fig. 5 Impact of angle restriction and vessel termination. Fifty networks were simulated for different sets of parameters to estimate average vessel length, branching angles, number of vessels, vessel termination, and distance from terminated vessels to the placenta boundary. Here, our first growth mechanism with the growth fraction, $t = 0.5$, is used

Thus, a larger growth fraction alone cannot explain all the structural features of placental vascular networks in at-risk individuals.

Vessel Lengths L_g Our second growth mechanism uses average vessel lengths chosen to empirically match at-risk and control groups, and so by design, agrees with the data for average vessel lengths (compare vessel lengths in Fig. 4 against

Fig. 2c). However, unlike our previous growth mechanism, longer vessel lengths in the at-risk group increases the percentage of branches terminated at early generations, leading to fewer vessels in the entire network. This additional termination arises because longer vessels are more likely to leave the convex hull of its seed set, thereby terminating the branching process. In other words, when vessel length is independent from its distance to a seed set's centroid, longer branches can cause early termination, a feature characteristic of at-risk individuals. At the same time, longer branches led to slightly wider branching angles and little difference in the distance from terminated vessels to placenta boundary, contrary to what is observed in at-risk individuals. So, like the previous growth mechanism, longer vessels alone cannot explain all the structural features of placental vascular networks in at-risk individuals.

Vessel Angles The angle between a vessel and each of its branches could be controlled by either the restriction angle θ or the angle reduction factor f . As illustrated in Fig. 3, networks with different restriction thresholds (left versus right) appear to have few visible changes for lower growth factors (top panels). Different restriction thresholds for higher growth factors, however, do appear to produce larger total rotation angles along any path through the network. For example, in the bottom left panel, the maximum total rotation angle can be visually estimated to be around 2π , while in the bottom right panel, there are many instances in which branches build up a total rotation of over 3π .

Using f to restrict the angle between a vessel and its branches also had little impact on either vessel length or branching angles in our analysis of averages over 50 networks (Fig. 5). This restriction did, however, have a slight impact on terminating the branching process, whereby more control of the branching angle ($f = 1$) leads to more terminated vessels and fewer vessels in total compared to less control ($f = 0.6$) cases. More angle control forces a vessel to deviate from its path to its seed set centroid. Similar to the case of longer vessels, additional termination arises because vessels are more likely to leave the convex hull of their seed sets.

Termination Clearly, a higher termination fraction α increases the number of vessels that are terminated (Fig. 5); However, a higher termination fraction α also increases vessel lengths at later generations in the case of our first growth mechanism. Longer vessels help compensate for the additional termination by allowing the vascular network to reach seed points that the terminated branches were supposed to reach. Note that terminating branches would not impact vessel length in the case of our second growth mechanism, since vessel lengths are set independently from the rest of the growth process. Unfortunately, a higher termination fraction led to little changes in branching angles, larger distances from the terminated vessels to the boundary, and vessel lengths at early generations. Therefore, termination alone cannot explain all the structural features of the placental vascular networks in the at-risk individuals.

3 Modeling Blood Flow in Placental Vascular Networks

We follow up the preceding section by exploring how a vascular network's structure influences its ability to transport blood. For simplicity, we consider the network to be an arterial vascular network and assume the venous network grows parallel to it, connecting the arterial network to the venous network at their terminal points. Hence, terminal points in the theoretical network becomes branching points and the new network has only one inlet and one outlet. We further assume the original terminal points mark approximate locations of the chorionic villi, where oxygen is transferred from maternal blood to fetal blood. This idealization allows us to dramatically reduce the number of boundary conditions needed to model blood flow and pressure. We then compared blood flow and pressure in these networks to study how parameters that influenced network structure, in turn, influenced blood flow and pressure. Section 3.1 introduces our mathematical model of the blood flow and pressure through the network and Sect. 3.2 shows our measures for quantifying the network's efficiency. Lastly, Sect. 3.3 presents numerical results from different types of simulated vascular networks.

3.1 Blood Flow and Pressure in a Vascular Network

For a single vessel, we relate volumetric blood flow rate F to pressure P_a and P_b at the vessel's ends. Assuming blood is a Newtonian fluid and flow is laminar, Krenz et al. [10] used Poiseuille's law to derive a simple relation between pressure and flow:

$$\mathcal{B}(P_a) - \mathcal{B}(P_b) = rF, \quad (5)$$

where $\mathcal{B}(P)$ is the anti-derivative of $h(P)^4$ with $h(P)$ determining how much a vessel distends, or expands, as a function of the pressure P (see Appendix 2 for details). Specifically, function $h(P)$ relates vessel diameter d under pressure P and vessel diameter d_0 under no pressure:

$$d = d_0 h(P). \quad (6)$$

The constant r is a constant called the resistance coefficient and is given by

$$r := \frac{128\mu L}{\pi d_0^4},$$

where L is vessel length, and $\mu = 2.084$ mPa·s (or 15.6×10^{-6} mmHg · s) is blood viscosity. Lastly, we assume vessels share a simple distensibility function $h(P)$:

$$h(P) := 1 + \beta P, \quad (7)$$

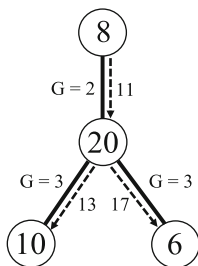


Fig. 6 Relationship between blood flow and pressure for a labeled branch point. The number inside the circle is the index for the node. The number next to the arrow is the index for the vessel. Generation number, G , is used to imply the flow direction; blood flows from lower to higher generation. In this case, the blood flow always flows from vessels with generation 2 to vessels with generation 3

for constant $\beta = 0.02 \text{ mmHg}^{-1}$.

We extend this model to a vascular network with n nodes and m vessels. Denote the pressure at the i th node by P_i and the blood flow rates in each of the m vessels by F_j . From Eq. (5), we have a linear equation in $\mathcal{B}(P_1), \dots, \mathcal{B}(P_n)$ and F_1, \dots, F_m for each of the m vessels. Our one-inlet-one-outlet network model implies that flow is conserved at every node except the two nodes representing the inlet and outlet, providing an additional $n - 2$ linear equations. With two boundary conditions for pressure: one at the inlet node and another at the outlet node, we can establish a linear system of $m + n$ equations in $m + n$ unknowns

$$A\mathbf{x} = \mathbf{b}, \tag{8}$$

where

$$\mathbf{x} = [\mathcal{B}(P_1), \mathcal{B}(P_2), \dots, \mathcal{B}(P_n), F_1, F_2, \dots, F_m]^T.$$

Upon solving Eq. (8) for \mathbf{x} , we recover flows F_1, \dots, F_m through each vessel immediately. We can use the inverse of $\mathcal{B}(P) = \frac{1}{5\beta}(1 + \beta P)^5$:

$$P = \mathcal{B}^{-1}(\mathcal{B}(P)) = \frac{(5\beta\mathcal{B}(P))^{\frac{1}{5}} - 1}{\beta},$$

to recover pressures P_1, \dots, P_n from $\mathcal{B}(P_1), \dots, \mathcal{B}(P_n)$.

To illustrate how to obtain the equations in (8), consider, for example, a localized structure in Fig. 6. For node 20, flow is conserved which yields the equation:

$$F_{11} - F_{13} - F_{17} = 0.$$

For vessels 13 and 17, applying Eq. (5) gives

$$\mathcal{B}(P_{20}) - \mathcal{B}(P_{10}) = r_{13} F_{13}, \quad \text{and}$$

$$\mathcal{B}(P_{20}) - \mathcal{B}(P_6) = r_{17} F_{17}.$$

3.2 Measures of Network Efficiency

With a model for blood flow and pressure, we want to measure a network’s efficiency in transporting oxygen and nutrients from maternal blood to the fetus. To this end, we consider the following three measurements:

Total flow rate through the network $\mathcal{F} := \sum_{i \in I_{in}} F_i$,

Average flow rate per “capillary” $\mathcal{F}_{cap} := \mathcal{F}/N$, and

Total volume of the network $\mathcal{V} := \sum_{i=1}^m V_i$.

Here, I_{in} is the set of indices for vessels connected to the inlet node, V_i is the volume of the i th vessel, and N is the number of terminal nodes in the arterial network before mirroring, where we assume the number of terminal nodes approximates the number of capillaries. Because vessels distend under pressure, the volume of each vessel also increases under pressure. Under the same assumptions used to derive our linear equations for blood flow and pressure, we can derive an expression of the volume of vessel i (see Appendix 2 for the derivation):

$$V_i = \frac{\pi d_0^2 L}{4} \frac{\left[\frac{1}{7}(1 + \beta P_{a_i})^7 - \frac{1}{7}(1 + \beta P_{b_i})^7 \right]}{\left[\frac{1}{5}(1 + \beta P_{a_i})^5 - \frac{1}{5}(1 + \beta P_{b_i})^5 \right]},$$

where P_{a_i} and P_{b_i} are pressures at the ends of vessel i . Note, volume is expressed as the volume under no pressure scaled by a dimensionless term that increases with increasing pressure.

We naturally consider the total flow rate \mathcal{F} as a measure of interest, since a greater flow rate is generally expected to translate to a greater rate of oxygen and other nutrients transferred from the maternal blood to the fetus. However, the transfer of oxygen and other nutrients depends on other aspects of the vascular network as well. Particularly, the vessels we considered in the networks would be connected to smaller vessels (capillaries) in a real placenta, called villi trees, where

the transfer of oxygen and nutrients actually occurs. Since we do not model villi trees explicitly, we make the simplifying assumption that these villi trees occur around the terminal nodes, or ends, of our arterial network. We also reason that the transfer of oxygen at each of these locations depends on the local flow rate. For this reason, we also consider the average flow rate per “capillary,” \mathcal{F}_{cap} , as a measure of local flow rates and a proxy for network efficiency as a whole.

Finally, we also consider the total volume \mathcal{V} of the network, since the metabolic power required to maintain the network is usually considered to be proportional to its volume. The use of volume in evaluating a vessel’s efficiency can be traced back to the seminal work of Murray [12], who related the radii of a parent vessel to its children vessels by assuming a vessel is designed to minimize work. Considering volume in addition to flow rates helps us evaluate the trade-off between transporting more blood easily versus meeting metabolic needs.

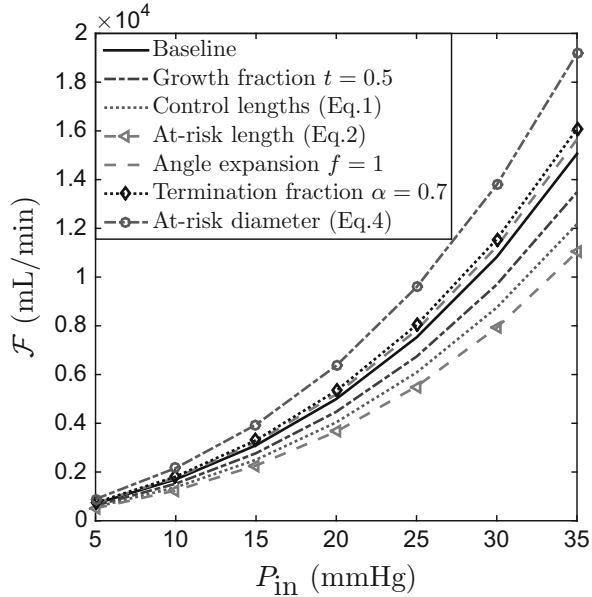
3.3 Results of the Impact of Vascular Growth on Blood Flow and Pressure

To examine how vascular growth influences blood flow, we constructed one-inlet-one-outlet networks using the same 50 networks generated for each of the seven parameter sets in Table 1 of Sect. 2.4. We then simulated blood flow through the network keeping the pressure P_{out} at the outlet node at zero and varying the pressure P_{in} at the inlet node. We found that total flow rate \mathcal{F} increased nonlinearly with increasing pressure P_{in} applied to the inlet of each vascular network. Figure 7 illustrates this nonlinearity for simulated networks corresponding to the seven parameter sets in Table 1. For each applied pressure P_{in} , the highest total flow rate was observed in networks with at-risk diameters followed by, in decreasing order of total flow rate, networks with greater termination ($\alpha = 0.7$), greater angle reduction ($f = 1$), baseline parameters, higher growth fraction ($t = 0.5$), control lengths, and at-risk vessel lengths.

From this ordering, we can see that networks with longer vessels had lower flow rates through the network. For example, four types of networks targeted vessel length: baseline (a growth fraction of $t = 0.4$), a growth fraction of $t = 0.5$, control vessel lengths, and at-risk vessel lengths. Total flow decreased in these four network types in the same order of increasing vessel length. From Eq. (5), we observe that longer vessels impact flow rates by increasing the resistance (r) in each vessel, thereby decreasing the flow in each vessel and subsequently, the total flow through the network. Put differently, since we impose the same difference in pressure across the whole network, the pressure difference per unit length is lower in networks with longer vessels, leading to slower flow rates.

In contrast to vessel length, increasing vessel diameter increased total flow rate through the network. This feature can be seen by comparing networks with vessel diameters determined from individuals at-risk for ASD to our baseline networks

Fig. 7 Total flow rate in the seven simulated networks with inlet pressure P_{in} ranged from 5 to 35. The network types are distinguished in the legend based on how they differ from baseline

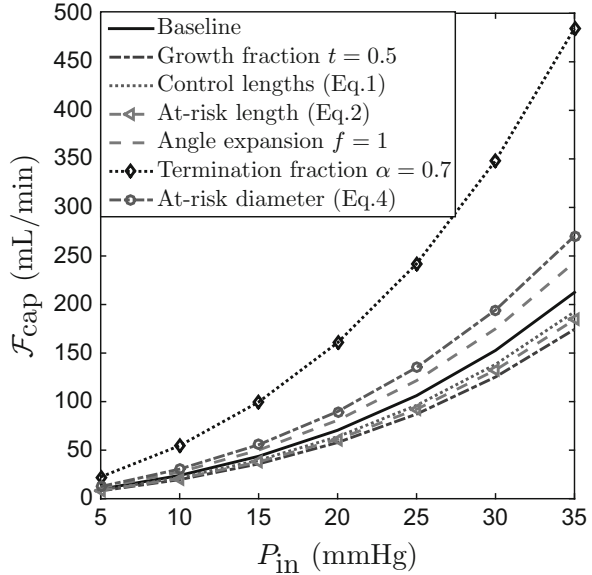


which had diameters determined from the controls (Fig. 7). Specifically, networks with at-risk diameters had thicker vessels and higher flow rates than networks with control diameters. Again, Eq. (5) explains this effect: thicker vessels have lower resistance (r) in each vessel, thereby increasing the flow in each vessel and subsequently, the total flow through the network. Resistance, however, is inversely proportional to vessel radius raised to the *fourth* power and directly proportional to vessel length. So even though at-risk individuals differ from controls relatively more in vessel length than vessel radius, these differences have comparable impacts on flow rates.

Compared to vessel length and diameter, vessel termination and controlling branching angles had a lesser impact on flow rates. In both cases, greater termination or greater restriction of large changes in flow direction led to a slight increase in flow. Even though branching angles do not directly impact the blood flow and pressure model, we found in Sect. 2.4 that greater control of branching angles led to more vessels being terminated. This result would suggest that any vessel termination, regardless of the exact mechanism, can increase flow rates.

Figure 8 considers our second measure of network efficiency: average flow rate per “capillary” \mathcal{F}_{cap} . For this measure, we find that longer vessels also lead to lower average flow rates \mathcal{F}_{cap} . Namely, average flow rates \mathcal{F}_{cap} decreased in the four network types targeting vessel length in the same order of increasing vessel length. We had already seen that vessel length can impact vessel termination, which in turn determines how many terminal nodes are in the arterial network. Thus, the impact of vessel length on total flow outweighs its impact on the number of terminal nodes, so that longer vessels lead to larger average flow rates, \mathcal{F}_{cap} . Thicker vessels

Fig. 8 Average flow per capillary in the seven simulated networks with inlet pressure P_{in} varied from 5 to 35

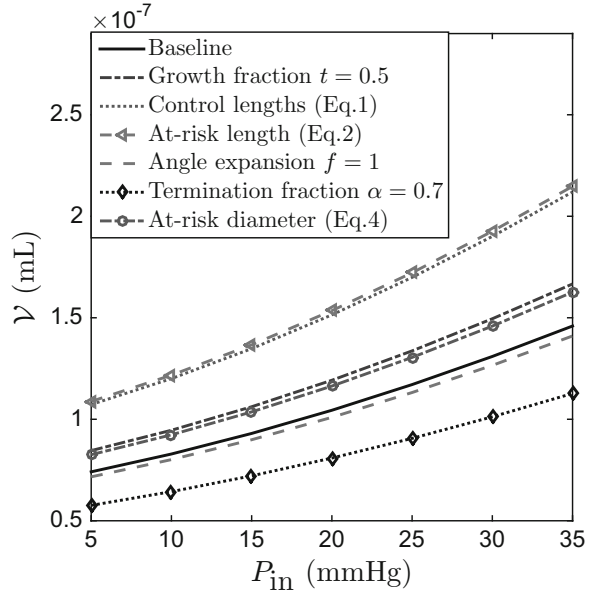


also increase average flow rates, \mathcal{F}_{cap} ; because again, this feature's impact on total flow rate outweighs its impact on the number of terminal nodes which is nil.

Vessel termination also has a large impact on average flow rates, \mathcal{F}_{cap} . In this case, greater vessel termination ($\alpha = 0.7$) leads to both fewer terminal nodes and a minimal increase in total flow, \mathcal{F} , which when taken together leads to higher average flow rates. Similarly, greater control of branching angles ($f = 1$) leads to slightly fewer terminal nodes and a minimal increase in total flow, \mathcal{F} , thereby leading to higher average flow rates. Since these higher average flow rates arise by ways of greater termination, greater control of branching angles does not have the same level of impact on average flow rates as simply increasing vessel termination directly.

Lastly, Fig. 9 shows the results on the total volume of the network, \mathcal{V} . As was expected, both longer and thicker vessels lead to a larger network volume, \mathcal{V} , indicating that networks with these features are more difficult to maintain metabolically. Early vessel termination, on the other hand, leads to a smaller network volume, making such network easier to maintain metabolically. When considering the volume along with the total flow, we observe that vessel termination and vessel radius could both be modified to balance an increase in total flow rates with an increase in network volume. Increasing vessel length, however, increases network volume while decreasing total flow, raising questions as to whether a network benefits from longer vessels. One possible benefit is that longer vessels had better network coverage to the boundary of the placenta, as we saw in the section on vascular growth. Perhaps, better coverage could mean less competition between branches for resources and more efficient oxygen transfer. Alternatively,

Fig. 9 Total volume in the seven simulated networks with P_{in} varied from 5 to 35



longer vessels are accompanied by thicker vessels in individuals associated with an enriched risk for ASD; each feature could compensate for the other by having opposite effects on total flow, and if compensated correctly, could balance the increase in total volume. These hypotheses, among others, should be studied further.

4 Discussion

In this project, we used mathematical modeling to explore how certain conditions during fetal development could increase the risk for autism in the newborn, via abnormal growth and function of placenta chorionic surface vascular networks. We first investigated potential mechanisms for growing vascular networks that are characteristic of at-risk for ASD, focusing on three candidate mechanisms: vessels grow longer/faster, vessel terminate more frequently before branching, or angles between connected vessels are more tightly controlled. We aimed to identify mechanism(s) that could reproduce empirical differences between individuals at-risk for ASD and controls including higher termination rates of vessels, longer vessels, lower total rotation angles along a vessel trajectory (to mimic tortuosity), and greater distances from terminals to the placental boundary. We then studied how structural properties of vascular networks impact blood flow through the network to determine if overall ability of the placenta to deliver appropriate oxygen and nutrients to the fetus is weakened in networks more characteristic of at-risk for ASD.

On the one hand, we noted that vessels grown more quickly, represented in our model by a higher growth fraction, led to networks with longer vessels and increased coverage to the placenta boundary (consistent with that observed in at-risk individuals), but also with wider branching angles and fewer terminated vessels (contrary to what is observed for at-risk individuals). On the other hand, we found that directly growing vessels longer leads to greater termination rates and fewer vessels, but also wider branching angles and little change to distances from terminated vessels to placenta boundary. Hence neither growth mechanism could explain in and of itself the observed differences between at-risk and control placental vascular networks. Meanwhile, tighter control of branching angles between vessels was found to both decrease total rotation (tortuous aspect) of the vessels to various degrees depending on other factors (such as growth speed) and to increase termination rates caused by increasing the number of vessels forced to leave the seed convex hull, but had little impact on other structural properties. So, while controlling branching angles may still be a crucial contributor, our results suggest that this mechanism also cannot be solely held accountable for the differences between at-risk and control placentas.

We conclude that a combination of these mechanisms or possibly others not considered in this study, rather than any of them in isolation, are needed to accurately capture empirical differences between individuals at-risk for ASD and controls. For example, placental tissue that is too stiff or fibrous could lead vessels to grow longer before finding tissue that is suitable for terminating or branching in ways that barely change flow directions since fibrous tissues often have preferential directions. This example shows how different mechanisms in vascular growth, via a common factor—tissue stiffness—could combine to generate vascular networks more characteristic of at-risk for ASD. Alternatively, vessel thickness may be a driving mechanism during vascular growth for similar reasons: thicker vessels could be more resistant to branching, so they terminate early or branch in ways that change very little in flow directions. Interestingly, vessel thickness is the only structural property we considered that differs significantly in the first generation of vascular networks between at-risk individuals and controls.

Regarding network function, our results showed that structural properties of at-risk individuals are able to compensate for each other's impact on network efficiency. That is, certain properties such as vessel length weaken network efficiency, whereas others such as termination rates improve network efficiency. In sum, we cannot definitely say whether vascular networks characteristic of at-risk individuals have a weaker ability to deliver appropriate oxygen and nutrients to the fetus. As such, it is unclear from our analysis alone if impaired network function is a contributing factor for being at-risk for ASD.

To arrive at these conclusions, we compared statistical measures related to blood flow and pressure in one-inlet-one-outlet vascular networks obtained by mirroring simulated vascular networks and connecting the two networks at their terminated vessels. These one-inlet-one-outlet networks were designed to capture a venous network that is parallel to an arterial network. We considered the impact of vascular growth and structural properties on three specific measures of network efficiency.

First, network flow rate was measured, since it is likely to be associated with rates of oxygen and nutrient transfer to the fetus. Second, average flow rate per “capillary” (terminated vessel) was measured to serve as a proxy for local flow rates in villi trees. These villi trees were not explicitly modeled, but are locations where oxygen and nutrients actually transfer from maternal blood to fetal blood, hence should depend on local flow rates. Third, total volume of blood in the network was measured due to its connection to metabolic cost for maintaining the entire vasculature. Indeed, the seminal work by Murray [12] balanced total volume in a vessel with transport power to determine optimal rules for radii of branching vessels.

From this analysis on blood flow, we found that with respect to all three measures longer branches led to less efficient networks, i.e., slower flow rates, measured in total and per capillary, but greater blood volume. Greater termination rates of vessels either captured directly in our growth model or indirectly through tighter control on branching angles, led to faster flow rates, especially average flow rates per capillary, and lower volumes—possibly acting to compensate for decreased flow rates due to longer vessels in high risk individuals. Meanwhile, thicker vessels, particularly those from at-risk individuals, have opposing impacts on network efficiency: greater flow rates, but lower volumes. In sum, termination rates, vessel length, and vessel thickness can be modified together to balance higher costs (greater blood volume) with better benefits (faster flow rates) in both controls and at-risk individuals, despite structural differences in their placentas. Put differently, some of the observed structural differences could arise to *prevent* changes in network efficiency.

In the current study, we made a number of simplifying assumptions, providing opportunities to further explore structural and functional properties of placental vascular networks. We focused primarily on only two branches in the first generation of vascular growth and on a centrally inserted umbilical cord, but these two properties may be crucial for the development of a vascular network. Umbilical cord position relative to the placenta is determined by the folding process of the fetus and by its position at the time of attachment to the wall of the placenta [8]. Moreover, vessels in actual placentas almost always branch into two vessels, except in the first generation step of the branching process, which can lead to anywhere from one to four branches. A centrally inserted umbilical cord is a reasonable assumption based on research studies in [3, 26], but in the future, it would be interesting to investigate these assumptions more carefully, as evidenced by [17, 27]. We also modeled the placenta as a disc and point an interested reader to papers [7, 24] for an investigation into how the region’s shape affects network structure during vascular growth.

In addition to exploring other mechanisms of vascular growth, future work could also consider other ways to evaluate network efficiency [9, 21, 23]. Gill et al. [9] suggest rates of oxygen and nutrient transport depend on both local flow rates and local geometry (e.g. cross-sectional area of vessels). Consequently, thicker vessels may lose some of their efficiency. We could also model villi trees explicitly such as done in [21] and elsewhere, since oxygen and nutrient transport occurs in these trees. Alternatively, Xia et al. [25] used a mathematical approach known as optimal transport to explain how structural changes in at-risk individuals could lead to inefficient transport of oxygen, nutrients, and biochemicals to the fetus. Another

possibility is to evaluate the spatial distribution of terminated vessels, e.g., using diffusion models, since more evenly distributed terminated vessels may diminish competition for resources between branches. Vessels that grew more quickly, for instance, had greater coverage to the placenta boundary and diminished competition during vascular growth in our model. Subsequently, these networks could have reduced competition for resources, leading to greater network efficiency. Finally, once the more refined selection of candidate key parameters, network measures, and candidate mechanisms relating these are in place, one could be developing efficient algorithms to perform a global sensitivity analysis of the system's behavior on these parameters.

While we are far from a single cohesive explanation for the role of placenta chorionic surface vascular networks in ASD risk, we provided an extensive and systematic investigation of candidate mechanisms for vascular growth in ASD risk, linking vascular growth to network structure and network structure to function. Our modeling framework provides a foundation for future endeavors on placental vascular networks in ASD risk. We highlighted a few hypotheses to examine more closely and a few ways to extend our work.

Acknowledgements The work described in this chapter was initiated during the Association for Women in Mathematics collaborative workshop Women Advancing Mathematical Biology hosted by the Mathematical Biosciences Institute (MBI) at Ohio State University in April 2017. Funding for the workshop was provided by MBI, NSF ADVANCE “Career Advancement for Women Through Research-Focused Networks” (NSF-HRD 1500481), Society for Mathematical Biology, and Microsoft Research.

Appendix 1: Coupled Growth of Placenta and Chorionic Vascular Tree

Figure 10 simulates the boundary of a growing placenta.

Appendix 2: Derivation of Vessel Volume

Poiseuille equation gives the following relation:

$$\frac{dP}{dL} = -\frac{128\mu}{\pi d^4} F. \quad (9)$$

If we assume all vessels share the common diameter-pressure relationship (vessel distensibility relationship):

$$\frac{d}{d_0} = h(P),$$

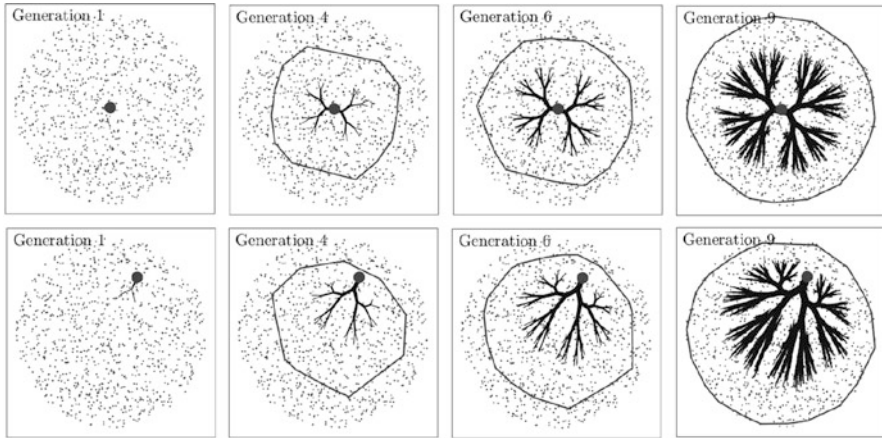


Fig. 10 Coupled growth of placenta and chorionic vascular tree. Left to right: generations 1, 4, 6, and 9 of the growth algorithm, with the diameter of the placenta gradually covering more of the given seed set. With this construction, the final distance between the vascular terminals and the boundary of the placenta is controlled by the growth rate t . The top versus the bottom panels illustrate the process for a central versus a random insertion of the umbilical cord, respectively. For the bottom panels, the growth algorithm was slightly altered to be initiated with a step of linear growth towards the centroid (aimed to reduce the distance caused by lack of centrality), preceding the first branching step

then integrating Poiseuille equation (9) from the start point to the end point of the vessel gives

$$\int_{P_a}^{P_b} (h(P))^4 dP = -rF \quad \text{and} \quad r = \frac{128\mu L}{\pi d_0^4}.$$

For convenience, define $\mathcal{B}(P)$ as the anti-derivative of $h(P)^4$. The equation above can be reduced as a linear drop of transformed pressure through the vessel [10].

$$\mathcal{B}(P_a) - \mathcal{B}(P_b) = rF. \tag{10}$$

In this paper, we consider the special case when $h(P) = 1 + \beta P$ so that $\mathcal{B}(P) = \frac{1}{5\beta} (1 + \beta P)^5$. Using this form of $\mathcal{B}(P)$, the vessel volume for each vessel, V_i , can be derived as follows:

$$\begin{aligned} V_i &= \int_0^L \frac{1}{4} \pi d^2 dL \\ &= \int_{P_a}^{P_b} -\frac{\pi^2 d^6}{4 \times 128\mu F} dP \\ &= \int_{P_a}^{P_b} -\frac{L\pi d_0^2}{rF} h^6(P) dP \end{aligned}$$

$$\begin{aligned}
&= \frac{L\pi d_0^2}{4rF} \frac{1}{7\beta} [(1 + \beta P_a)^7 - (1 + \beta P_b)^7] \\
&= \frac{L\pi d_0^2}{4} \frac{\frac{1}{7} [(1 + \beta P_a)^7 - (1 + \beta P_b)^7]}{\frac{1}{5} [(1 + \beta P_a)^5 - (1 + \beta P_b)^5]}.
\end{aligned}$$

Notice that we substituted in Eq. (9) in the second step and Eq. (10) was used in the last step.

References

1. G.M. Anderson, Autism biomarkers: challenges, pitfalls and possibilities. *J. Autism Dev. Disord.* **45**(4), 1103–1113 (2015)
2. A. Angelidou, S. Asadi, K.-D. Alysandratos, A. Karagkouni, S. Kourembanas, T.C. Theoharides, Perinatal stress, brain inflammation and risk of autism-review and proposal. *BMC Pediatr.* **12**(1), 89 (2012)
3. J.-M. Chang, A. Mulgrew, C.M. Salafia, Characterizing placental surface shape with a high-dimensional shape descriptor. *Appl. Math.* **3**, 954–968 (2012)
4. J.-M. Chang, H. Zeng, R. Han, Y.-M. Chang, R. Shah, C.M. Salafia, C. Newschaffer, R.K. Miller, P.J. Katzman, J. Moye, M. Fallin, C.K. Walker, L. Croen, Autism risk classification using placental chorionic surface vascular network features. *BMC Med. Inform. Decis. Mak.* **17**(1), 162 (2017)
5. A.R. Clark, M. Lin, M. Tawhai, R. Saghian, J.L. James, Multiscale modelling of the fetoplacental vasculature. *Interface focus* **5**(2), 20140078 (2015)
6. C. Costa, J. Incio, R. Soares, Angiogenesis and chronic inflammation: cause or consequence? *Angiogenesis* **10**(3), 149–166 (2007)
7. S.L. Cotter, V. Klika, L. Kimpton, S. Collins, A.E.P. Heazell, A stochastic model for early placental development. *J. R. Soc. Interface* **11**(97), 20140149 (2014)
8. K. Coward, D. Wells, *Textbook of Clinical Embryology* (Cambridge University Press, Cambridge, 2013)
9. J.S. Gill, C.M. Salafia, D. Grebenkov, D.D. Vvedensky, Modeling oxygen transport in human placental terminal villi. *J. Theor. Biol.* **291**, 33–41 (2011)
10. G.S. Krenz, C.A. Dawson, Flow and pressure distributions in vascular networks consisting of distensible vessels. *Am. J. Physiol. Heart Circ. Physiol.* **284**(6), H2192–H2203 (2003)
11. U. Meyer, J. Feldon, O. Dammann, Schizophrenia and autism: both shared and disorder-specific pathogenesis via perinatal inflammation? *Pediatr. Res.* **69**(5 Pt 2), 26R (2011)
12. C.D. Murray, The physiological principle of minimum work: I. The vascular system and the cost of blood volume. *Proc. Natl. Acad. Sci.* **12**(3), 207–214 (1926)
13. C.J. Newschaffer, L.A. Croen, M.D. Fallin, I. Hertz-Picciotto, D.V. Nguyen, N.L. Lee, C.A. Berry, H. Farzadegan, H.N. Hess, R.J. Landa, S.E. Levy, M.L. Massolo, S.C. Meyerer, S.M. Mohammed, M.C. Oliver, S. Ozonoff, J. Pandey, A. Schroeder, K.M. Shedd-Wise, Infant siblings and the investigation of autism risk factors. *J. Neurodev. Disord.* **4**, 1–16 (2012)
14. P.H. Patterson, Maternal infection and immune involvement in autism. *Trends Mol. Med.* **17**(7), 389–394 (2011)
15. D.A. Rossignol, R.E. Frye, A review of research trends in physiological abnormalities in autism spectrum disorders: immune dysregulation, inflammation, oxidative stress, mitochondrial dysfunction and environmental toxicant exposures. *Mol. Psychiatry* **17**(4), 389 (2012)

16. C.M. Salafia, Placental vascular tree as biomarker of autism/ASD risk. Annual report for U.S. Army Medical Research and Materiel Command at Fort Detrick, Maryland 21702-5012 W81XWH-10-1-0626, Research Foundation for Mental Hygiene (2014), <http://www.dtic.mil/dtic/tr/fulltext/u2/a575079.pdf>.
17. C.M. Salafia, M. Yampolsky, D. Misra, O. Shlakhter, D. Haas, B. Eucker, J. Thorp, Placental surface shape, function, and effects of maternal and fetal vascular pathology. *Placenta* **31**, 958–962 (2010)
18. C.M. Salafia, T. Girardi, M. Yampolsky, O. Shlakhter, C. Newschaffer, D. Fallin, C. Walker, C. Stodgell, P. Katzman, J. Culhane, P. Landrigan, S. Szabo, N. Thieux, J. Swanson, N. Dole, M. Varner, J. Moye, R. Miller, Chorionic vascular structure and placental functional efficiency (beta) differ in high and low autism risk placental cohorts. *Placenta* **34**, A72 (2013)
19. C.M. Salafia, C. Platt, T. Girardi, R. Shah, G. Merz, D.P. Misra, Placental structure in ASD: does the placenta mirror the diagnosis? in *2014 International Meeting for Autism Research*, page Abstract No. 17578 (2014)
20. K. Sato, Placenta-derived hypo-serotonin situations in the developing forebrain cause autism. *Med. Hypotheses* **80**(4), 368–372 (2013)
21. A.S. Serov, C.M. Salafia, P. Brownbill, D.S. Grebenkov, M. Filoche, Optimal villi density for maximal oxygen uptake in the human placenta. *J. Theor. Biol.* **364**, 383–396 (2015)
22. C.Y. Wang, J.B. Bassingthwaighite, L.J. Weissman, Bifurcating distributive system using Monte Carlo method. *Math. Comput. Model.* **16**(3), 91–98 (1992)
23. Q. Xia, C. Salafia, Transport efficiency of the human placenta. *J. Coupled Syst. Multiscale Dyn.* **2**(1), 1–8 (2014)
24. Q. Xia, C.M. Salafia, S. Morgan, Optimal transport and placental function, in *Interdisciplinary Topics in Applied Mathematics, Modeling and Computational Science* (Springer, Berlin, 2015), pp. 509–515
25. Q. Xia, L.A. Croen, M.D. Fallin, C.J. Newschaffer, C. Walker, P. Katzman, R.K. Miller, J. Moye, S. Morgan, C. Salafia, Human placentas, optimal transportation and high-risk autism pregnancies. *J. Coupled Syst. Multiscale Dyn.* **4**(4), 260–270 (2016)
26. M. Yampolsky, C.M. Salafia, O. Shlakhter, D. Haas, B. Eucker, J. Thorp, Modeling the variability of shapes of human placenta. *Placenta* **29**, 790–797 (2008)
27. M. Yampolsky, C.M. Salafia, O. Shlakhter, D. Haas, B. Eucker, J. Thorp, Centrality of the umbilical cord insertion in a human placenta influences the placental efficiency. *Placenta* **30**, 1058–1064 (2009)